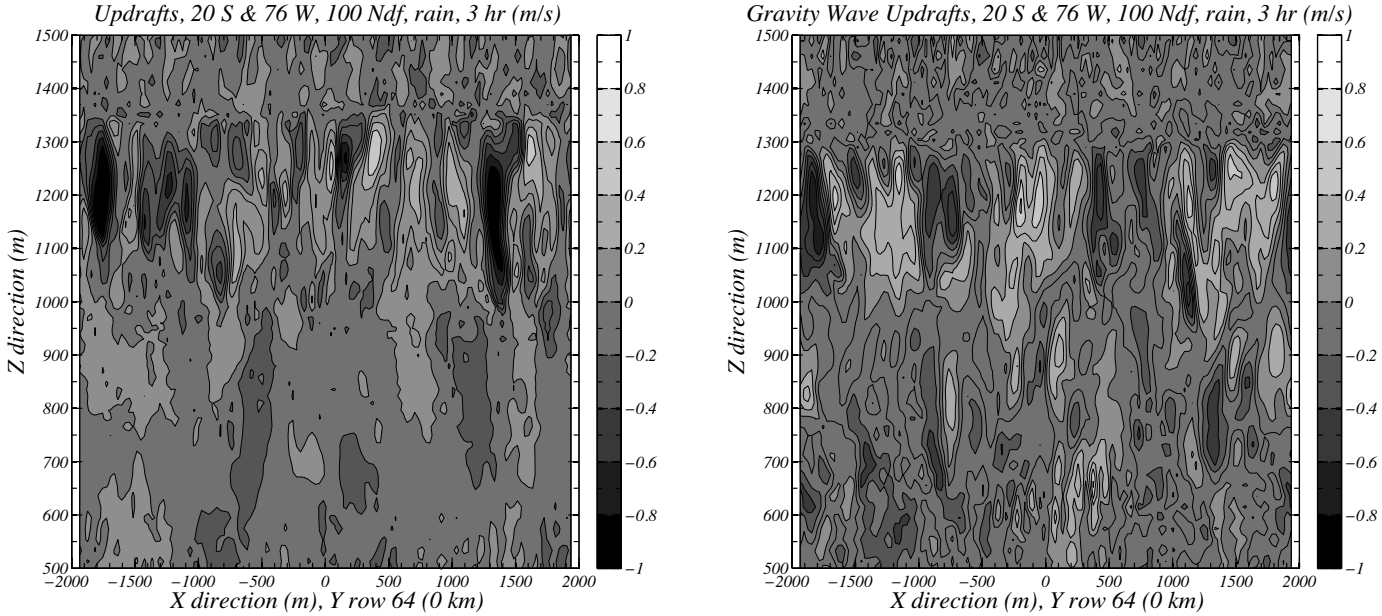

Figure 4 Vertical cross-section of LEM updraft velocity LEM field at 1100 local time on centred at 76 W, 20 S for left: no gravity wave; and right: immediately after simulated gravity wave.

The three dimensional structure and kinematics of drizzling stratocumulus, *Mon. Wea. Rev*., **135**, 3767–3784, 2007.

Derbyshire, S. H., A. R. Brown and A. P. Lock, The Meteorological Office Large-Eddy Simulation model, *Met O (APR) Turbulence and Diffusion Note* No. **213** (1994).

M. E. B. Gray, J. Petch, S. H. Derbyshire, A. R. Brown, A. P. Lock, H. A. Swann and P. R. A. Brown., Version 2.3 of the Met. Office Large Eddy Model: Part II. Scientific Documentation, *Met O (APR) Turbulence and Diffusion Note* No. **276** (2001).

Menzel, W. P., and J. F. YV. Purdom, Introducing GOES I: The first of a new generation of Geostationary Operational Environmental Satellites, *Bull. Am. Meteorol. Soc*., **75**, 757-781, 1994.

Minnis, P., et al., 1995: Cloud Optical Property Retrieval (Subsystem 4.3). "Clouds and the Earth's Radiant Energy System (CERES) Algorithm Theoretical Basis Document, Volume III: Cloud Analyses and Radiance Inversions (Subsystem 4)", *NASA RP 1376* Vol. 3, edited by CERES Science Team, pp. 135-176.

Sharon, T. M., Albrecht, B. A., Jonsson, H., Minnis, P., Khaiyer, M. M., VanReken, T. M., Seinfeld, J., and Flagan, R.: Aerosol and cloud microphysical characteristics of rifts and gradients in maritime stratocumulus clouds, *J. Atmos. Sci*., **63**, 983–997. 2006.

Stevens, B., Vali, G., Comstock, K., Wood, R., VanZanten, M., Austin, P. H., Bretherton, C. S., and Lenschow, D. H.: Pockets of Open Cells (POCs) and Drizzle in Marine Stratocumulus, *Bull. Am. Meteor. Soc*., **86**, 51–57, 2005.

Wood, R., Comstock, K. K., Bretherton, C. S., Cornish, C., Tomlinson, J., Collins, D. R., and Fairall, C.: Open cellular structure in marine stratocumulus sheets, *J. Geophys. Res*., **113**, doi:10.1029/2007JD009 596, 2008.

van Zanten, M. C., and B. Stevens, 2005: On the observed structure of heavily precipitating marine stratocumulus. *J. Atmos. Sci.*, **62**, 4327–4342.

Ship-based observation of drizzling stratocumulus clouds from EPIC to VOCALS

de Szoeke, S.P[1]., S.E. Yuter[2], P. Zuidema[3], C.W. Fairall[4], W.A. Brewer[5],
[1]Oregon State University, Corvallis, OR., [2]North Carolina State University, Raleigh, NC., [3]University of Miami, FL., [4]NOAA ESRL Physical Sciences Division, Boulder, CO., [5]NOAA ESRL Chemical Sciences Division, Boulder, CO. USA.
Corresponding author: sdeszoek@coas.oregonstate.edu

Extensive high-albedo marine stratocumulus clouds are found in the subtropical and tropical eastern oceans, where they have a strong cooling influence on the top-of-atmosphere and surface radiation budgets. Feedbacks among upwelling, sea surface temperature (SST), surface fluxes, and stratocumulus clouds are difficult for coupled general circulation models to simulate, resulting in SST errors greater than 1°C in parts of the southeastern tropical Pacific Ocean (de Szoeke et al., 2010). Although errors in coupled models for the region have been recognized for some time, the southeastern tropical Pacific was only sparsely observed before 2001.

Stratocumulus clouds were observed on seven NOAA research cruises to the southeastern tropical Pacific Ocean in 2001 and 2003-2008. The NOAA ship *Ronald H. Brown* was deployed on two research cruises in 2008 as part of the VAMOS Ocean Cloud Atmosphere Land Study (VOCALS) Regional Experiment. Each cruise traversed 20°S, 75-85°W, offshore of the Arica Bight between Peru and Chile. Several sensors were used in combination to observe marine atmospheric boundary layer clouds and precipitation during each cruis. Microwave radiometers measured the column water vapor and liquid water path (LWP, Zuidema, 2005). Laser ceilometers measured cloud base height and temporal cloud fraction. Radar wind profilers retrieved inversion height. Surface air temperature, humidity, and winds, as well as vertical fluxes of heat and humidity, were measured by instruments on a mast at the bow of the ship (de Szoeke et al., 2010). Radiometers measured downwelling solar and longwave thermal radiation. A scanning C-band radar measured reflectivity from precipitation-sized drops (Comstock et al., 2004). In 2001 and 2008, millimeter-wavelength radar profiled clouds above the ship.

On the VOCALS regional experiment in 2008, a new motion-stabilized sensitive W-band 3.2 mm cloud radar instrument provided for the first time a unique view of clouds, in-cloud turbulence, and drizzle for over 500 hours. Additionally, observations from the NOAA scanning high-resolution Doppler

lidar provided aerosol backscatter, mean horizontal wind, vertical wind, and surface mixing layer height estimates below the cloud (Tucker et al., 2009).

Seven years measuring marine stratocumulus in the southeastern tropical Pacific

A new synthesis data set contains SST, surface meteorology and radiation, upper-air profiles from rawinsondes, and air-sea flux measurements for eight research cruises along 20°S, 75-85°W in boreal fall in 7 years (2001, 2003-2008; de Szoeke et al., 2010). Macroscopic cloud properties are also summarized in the synthesis data set. Figure 1a shows cloud top and cloud base height, surface lifting condensation level (LCL), and liquid water path (LWP) averaged in 2.5° longitude bins for the eight cruises. Cloud top height is detected from vertically pointing cloud radar or inferred from either the boundary layer inversion height in radiosonde temperature profiles or 915 MHz wind profiler data. Stratocumulus cloud base height is measured optically by the ceilometer. Stratocumulus cloud base height data is filtered to minimize the effect of occasional cumulus clouds below the stratocumulus. Stratocumulus cloud base height and cloud top height increase toward the west by ~300m over 10° longitude, while cloud thickness is nearly unchanged. Surface LCL is nearly flat with longitude, yet the stratocumulus cloud base is higher to the west.

Mean LWP is about 75 g m^{-2} east of 80°W, and more than 100 g m-2 west of 80°W. Whiskers on the mean LWP are the standard error of the 10-minute data, assuming a decorrelation time scale of one hour. Cloud LWP is expected to be nearly quadratic with cloud thickness, with condensation of water vapor following the moist-adiabatic temperature profile in the cloud. Whether clouds are raining or not, columns were found to have LWP slightly below this adiabatic amount (Zuidema et al., 2005). Since mean stratocumulus cloud thickness does not increase westward, the LWP increase could be related to increasing liquid water content per unit volume within the cloud. Intermittent shallow cumulus clouds between the LCL and the stratocumulus cloud base could also explain higher LWP to the west.

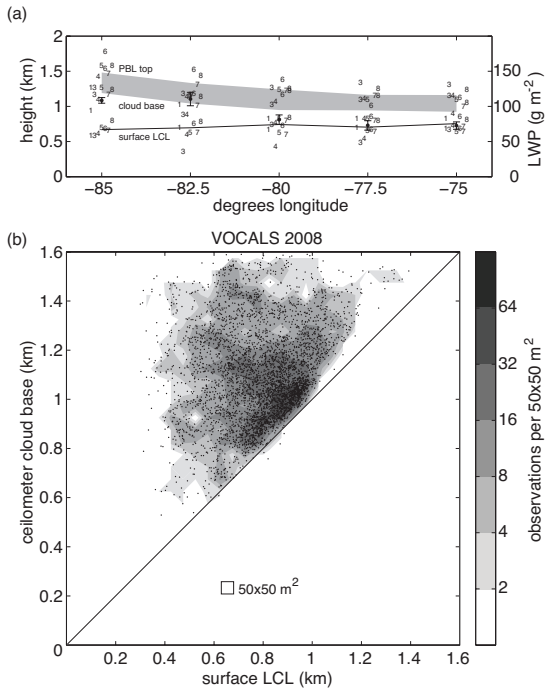

Figure 1. (a) Mean cloud base and top height (gray), and surface parcel lifting condensation level (LCL) in 2.5° longitude bins along 20°S, 75-85°W for all stratocumulus research cruises. The mean for each cruise year (2001, 2003-2008) is indicated by the last digit of the year (1, 2-8). Filled circles and whiskers show liquid water path (LWP). (b) Cloud base height measured by the ceilometer compared against surface LCL for VOCALS 2008. Clouds that condense above the surface LCL indicate the clouds are decoupled from the surface, or surface moisture is diluted by dry air in the boundary layer.

Figure 1b shows the surface LCL and ceilometer cloud base for each 10-minute average during VOCALS 2008. Cloud base is almost always observed above the LCL. The mode of the distribution corresponds to cloud base nearly 100 m above LCL. Cloud bases several hundred meters higher than LCL also occur, with 20% of cloud bases more than 500 m above the LCL. Since SST is warmer than the air, we expect a buoyancy-driven surface mixed layer, yet Figure 1b shows undiluted parcels from the surface often do not reach cloud base. Some soundings show conditionally unstable layers between the adiabatic surface layer and the moist-adiabatic cloud layer. Doppler lidar data collected in VOCALS can be employed to show the time-varying depth of turbulent mixing connected to the surface.

Enhanced radar observations of cloud and drizzle for VOCALS

In addition to the yearly observations of cloud boundaries, surface meteorology, and fluxes, two Doppler radars, a millimeter-wavelength W-band cloud radar and a centimeter-wavelength C-band precipitation radar, were deployed on the Brown.

The W-band radar pointed vertically and sampled the overlying column 3 times per second at 25-m vertical resolution. Sensitivity of the W-band radar was enhanced for the second VOCALS cruise leg so that it could detect cloud particles with reflectivity down to -30 dBZ.

Figure 2a shows W-band radar reflectivity, cloud top height, and cloud base height for November 12-15, when the ship was stationed at 75°W. Radar reflectivity is weak for clouds and stronger for drizzle. The ceilometer cloud fraction is 0.94 during the entire VOCALS cloud radar record. Of the clouds detected by the ceilometer, 14% are too weak to be detected by the cloud radar. Drizzle can be seen as high reflectivity that emerges below the cloud base. Drizzle detected near the surface is only a fraction of the times that there is drizzle at cloud base.

Examination of data from multiple years indicates that clouds have a strong diurnal cycle in cloud top height at 85°W, and a weak diurnal cycle at 75°W. This is explained by the diurnal vertical velocity perturbations of the "upsidence-wave", a gravity wave propagating offshore from its heat source in the Andes (Rahn and Garreaud, 2010). At 85°W the upsidence wave reinforces the typical diurnal cycle of nighttime deepening and daytime dissipation driven by solar radiation-modulated cloud-top entrainment. At 75°W the upsidence wave destructively interferes with the local diurnal cycle. As a result, at 85°W vertical velocity in the inversion varies with a strong diurnal component, while at 75°W, the diurnal component of vertical velocity is weaker and a semidiurnal component is present. VOCALS provides an unprecedented look at what actually happens to clouds and the boundary layer over the diurnal cycle.

The period from 12 UTC November 12 to 0 UTC November 15 shows variations at 75°W consistent with the diurnal cycle in cloud top height, cloud thickness, and radar reflectivity (Figure 2a). The LWP observed on November 12-15 (Figure 2b) was consistent with the long-term climatology from satellites (O'Dell et al., 2008). In Figure 2a clouds are higher and thicker at approximately 0 and 12 hours UTC (19 and 7 hours local, approximately 1 hour after sunset and sunrise). Radar reflectivity is higher within and below the cloud, indicating more intense clouds and drizzle when cloud tops extended to higher altitudes. Liquid water path variations from the microwave radiometer over November 12-15 also follow the cycles of cloud thickness and drizzle (Figure 2b). Adiabatic LWP (gray) depends only on the cloud thickness squared, and predicts the microwave-retrieved LWP (black) well.

Figure 2c shows a histogram of W-band radar column

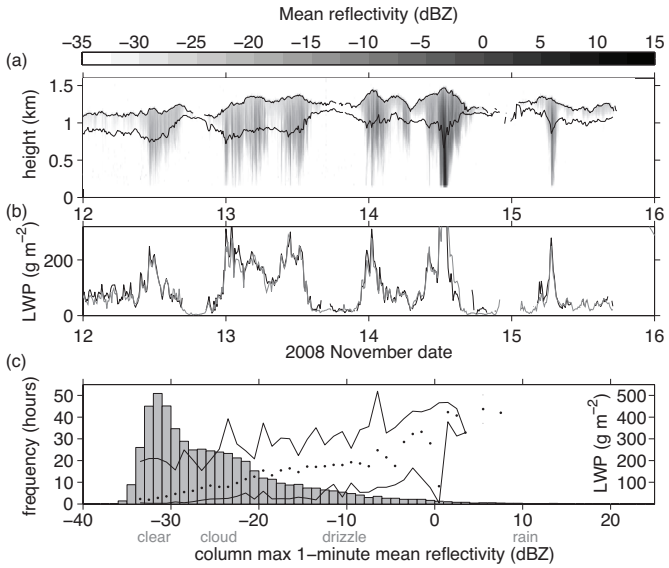

Figure 2. (a) Mean reflectivity from the W-band cloud radar for November 12-15, when the ship was near 20°S, 75°W. Thin lines are cloud top height estimated from the radar and cloud base height from the ceilometer. (b) Liquid water path (LWP) from the microwave instrument (black) and adiabatic LWP from cloud thickness (gray). There are two distinct peaks in cloud top, liquid water, and precipitation for each day, especially November 13-14. Bars in (c) show the frequency of occurrence in hours of column maximum reflectivity (dBZ) of 1-minute samples for all 538 hours of the VOCALS cloud radar record. The median and range of 10-minute LWP (g m-2, dots and lines) are binned by column maximum reflectivity.

maximum reflectivity (CMR) over all 538 hours the radar operated in VOCALS 2008. The 4-day period in Figs. 2a and b are a subset of these 538 hours. CMR is averaged over 1-minute intervals and counted in 1-dBZ wide reflectivity bins. Frequency of observing 1-minute mean CMR in each bin is given in hours. The mode of the distribution (-35 to -30 dBZ) represents clear-air noise and reflectivity too weak to exceed the level of instrumental noise. The distribution is positively skewed: 2% of minutes have CMR > -10 dBZ, 0.6% have CMR > 0 dBZ, 0.1% have CMR > 10 dBZ.

Liquid water path is composited within the 1-dBZ reflectivity bins. Dots in Figure 2c show the median LWP, and lines show the range of LWP found for each reflectivity bin. A linear fit of about 9 g m^{-2} per dBZ is reliable for clouds with weak (-35 to -20 dBZ) maximum reflectivity. The LWP-reflectivity relationship has weaker LWP dependence on CMR in the light drizzle regime of -20 to -10 dBZ. Columns with precipitation (0-10 dBZ) appear to contribute more strongly to LWP.

Columns with maximum reflectivity between -30 and -20 dBZ likely correspond to nonprecipitating clouds. A long tail of decreasing probability from -20 dBZ extends to about +10 dBZ. Column maximum reflectivity above -20 dBZ is associated with a distribution of Doppler velocities that is biased slightly downward, indicating that a subset of particles are large enough to fall and to be classified as precipitation. By about 0 dBZ columns almost certainly contain drizzle. Maximal reflectivity in a nonprecipitating cloud is probably found at cloud top, where the temperature is lowest and there is most condensate. Maximal reflectivity for a precipitating cloud is probably found at cloud base. Drizzle forms and falls out of the stratocumulus cloud and often re-evaporates before reaching the ground (cf. Figure 2a), thereby approximately conserving the combination of water vapor, liquid cloud, and rain water in the atmospheric column (Comstock et al., 2004).

The C-band radar scanned 60-km radius volumes and made four range-height scans along and across the prevailing wind direction every three minutes. Satellite images coincident with the volume scans show the pattern of clouds and their mesoscale organization. C-band radar volumes show the evolution of mesoscale precipitation structures within the clouds. Following the trend in the distribution of reflectivity from the W-band cloud radar, the distribution of C-band reflectivity is strongly skewed toward low values. The C-band radar fills in the higher ranges of reflectivity that the W-band cloud radar cannot observe. On a few occasions, small areas of precipitation greater than 40 dBZ were observed by the C-band radar. Scanning an 11 000 km^2 area continuously for more than 1000 hours, the C-band radar sampled mesoscale precipitation structure more than any other combination of instruments in the VOCALS regional experiment.

One hypothesis tested in VOCALS was whether drizzle is a necessary condition for the formation and maintenance of pockets of open-cell convection (POCs, Stevens et al., 2005). Precipitation observations from the C-band radar tell a subtler story. Cloud and precipitation images from satellite were classified into closed-cell conditions (unbroken clouds) or open-cell conditions (broken clouds). The C-band radar detects precipitation over the volume, so images can be categorized as drizzling or non-drizzling. Some open-cell scenes had drizzle, while other open-cell scenes had no C-band radar-detectable drizzle. Closed-cells were also observed both with and without C-band radar detectable drizzle. It is possible drizzle was present in open-cell clouds that was so light it could not be detected by the C-band radar. Unless cells pass directly over the ship, they cannot be observed by the vertically pointing W-band radar. Work is in progress to compare the statistics of the more sensitive W-band radar reflectivity over the ship with the C-band radar's less sensitive but wider-area measurements to assess the probability of missed drizzling echo under different cloudiness conditions.

Ship-based observations of clouds already provide valuable data for validating satellite products and numerical models over the southeastern tropical Pacific Ocean (e.g. Brunke et al., 2010). Further analysis of the observations will test the VOCALS hypotheses and refine our knowledge of cloud and precipitation processes in drizzling and non-drizzling stratocumulus clouds.

References

Brunke, M. A., S. P. de Szoeke, P. Zuidema, and X. Zeng, 2010: A comparison of ship and satellite measurements of cloud properties in the southeast Pacific stratus deck. *Atmos. Chem. and Phys. Disc*. in press.

Caldwell, P., C. S. Bretherton, and R. Wood, 2005: Mixed-lay budget analysis of the diurnal cycle of entrainment in southeast Pacific stratocumulus. *J. Atmos. Sci*. **62**, 3775-3791.

Comstock, K. K., R. Wood, S. E. Yuter, and C. S. Bretherton, 2004: Reflectivity and rain rate in and below drizzling stratocumulus. *Quart. J. Roy. Meteor. Soc*. **103**, 2891-2918.

de Szoeke, S. P., C. W. Fairall, D. E. Wolfe, L. Bariteau, P. Zuidema, 2010: Surface flux observations on the southeastern tropical Pacific Ocean and attribution of SST errors in coupled ocean-atmosphere models. *J. Climate*, submitted.

O'Dell, C. W., F. J. Wentz, and R. Bennartz, 2008: Cloud Liquid Water Path from Satellite-Based Passive Microwave Observations: A New Climatology over the Global Oceans. *J. Climate*, **21**, 1721-1739.

Rahn, D. and R. Garreaud, 2009: Marine boundary layer over the subtropical southeast Pacific during VOCALS-REx – Part 1: Mean structure and diurnal cycle. *Atmos. Chem. and Phys. Disc*. **9**, 26029-26062.

Stevens, B., G. Vali, K. Comstock, R. Wood, M. C. van Zanten, P. H. Austin, C. S. Bretherton, D. H. Lenschow, 2005: Pockets of open cells in and drizzle in marine stratocumulus. *Bull. Amer. Met. Soc*. **86**, 51-57. doi:10.1175/BAMS-86-1-51.

Tucker, S. C., and Coauthors, 2009: Doppler Lidar Estimation of Mixing Height Using Turbulence, Shear, and Aerosol Profiles. *J. Atmos. and Oceanic Tech*., **26**, 673-688.

Zuidema, P., E. R. Westwater, C. Fairall, and D. Hazen, 2005: Ship-based liquid water path estimates in marine stratocumulus. *J. Geophys. Res*. **110**, D20206. doi:10.1029/2005JD005833.